J. Fluid Mech. (1999), *vol.* 391, *pp.* 293–318. Printed in the United Kingdom

On the stability of liquid ridges

By R. VALÉRY ROY AND LEONARD W. SCHWARTZ

Department of Mechanical Engineering, University of Delaware, Newark, DE 19716, USA

(Received 17 June 1998 and in revised form 22 February 1999)

We consider the stability of a rectilinear liquid region whose boundary is composed of a solid cylindrical substrate of arbitrary shape and a free surface whose cross-section, in the absence of gravity, is a circular arc. The liquid–solid contact angle is a prescribed material property. A variational technique, using an energy functional, is developed that predicts the minimum wavelength for transverse instability under the action of capillarity. Conversely, certain configurations are absolutely stable and a simple stability criterion is derived. Stability is guaranteed if, for given substrate geometry and given contact angle, the unperturbed meniscus pressure is an increasing function of the liquid cross-sectional area. The analysis is applied to a variety of liquid/substrate configurations including (i) a liquid ridge with contact lines pinned to the sharp edges of a slot or groove, (ii) liquid ridges with free contact lines on flat and wedge-shaped substrates as well as substrates of circular or elliptical cross-section. Results are consistent with special cases previously treated including those that employ a slope-small-slope approximation.

1. Introduction

The problem of determining the shape and stability of capillary surfaces has a long and rich history. Capillary surfaces are of interest mathematically as surfaces of prescribed mean curvature, but more importantly because they appear in many natural and technological processes. The study of static capillary surfaces has applications in a wide variety of fields: in two-phase porous media flow (oil recovery), in the coating technologies, in integrated circuit technology, in respiratory mechanics (airways closure), etc. Microgravity environments have led to renewed interest in applications where the distribution of liquids is strongly affected by capillary forces: growth of crystals in liquid zones, other materials processing, design of spacecraft tanks which guarantee fuel outflow, etc. For excellent reviews of the historical development of capillary mechanics, or of the mathematical and physical background of interfacial surfaces, drops and bubbles, see Padday (1969), Princen (1969) and more recently Michael (1981). Significant progress has been made for the pendant and sessile drops maintained in equilibrium by a combination of surface tension and gravitational forces. See Padday & Pitt (1973), Concus & Finn (1979, 1990), Finn (1986).

It is well-known since the work of Plateau and Rayleigh that free liquid cylinders of circular cross-section are subject to capillary axial instabilities if the cylinder length exceeds its circumference. The same instability criterion applies to cylindrical liquid columns supported by coaxial circular disks, or for thin liquid linings of the interior or exterior of a cylindrical tube. Similar axial instabilities are known for other cylindrical liquid configurations, such as liquid 'fillets' pinned to a slot (Majumbar & Michael 1976; Brown & Scriven 1980), or static rivulets with free contact lines which partially

wet a flat substrate (Davis 1980), or the sidewalls of an edge or a wedge (Langbein 1990).

Here, we analyse the stability of cylindrical liquid ridges which partially wet an arbitrarily curved cylindrical substrate with a prescribed constant static contact angle. We assume that the equilibrium is achieved purely by a balance of interfacial forces at all solid–liquid, solid–vapour and liquid–vapour interfaces. Hence we neglect the influence of all body forces, so that the cross-section of the unperturbed equilibrium capillary surface is an arc of a circle. Our goal is to determine the conditions satisfied between the curvatures of the solid and liquid surfaces and the contact angle which guarantee stability of the cylindrical meniscus, and to predict, for unstable configurations, the critical wavelength for which all transverse disturbances of larger wavelength are destabilizing. If a cylindrical meniscus is unstable, it may break into separate droplets, and dewet some portion of the substrate.

The equilibrium conditions and stability properties of a capillary surface can be obtained by consideration of the difference in interfacial energies between the perturbed and unperturbed configurations. A general class of infinitesimal smooth perturbations is obtained by displacing each point of the unperturbed surface by a distance $\eta(s, z)$ along the surface normal direction, where s is the arclength measured along a cross-section, and z is measured along the axis of the cylindrical liquid surface. By letting the first variation of the energy to be zero for all small infinitesimal, volume-conserving perturbations, one obtains the classical Laplace and Young–Laplace equations governing the shape of a capillary surface bounding a specified liquid volume. Assuming these equations to hold, stability can then be guaranteed if the second-order energy variation remains positive for all volume-conserving perturbations. The problem then amounts to finding the minimal value reached by a quadratic functional $Q(\eta)$ on the set of smooth shape deformations η satisfying a volume constraint. The corresponding variational problem is known to be equivalent to the solution of an eigenvalue problem. This analysis shows that two possible modes of instability can occur: planar modes, i.e. independent of the z-coordinate, and transverse modes exhibiting sinuous variations along the z-direction.

Of most interest is to find the critical wavelength above which all sinuous transverse modes are destabilizing. The occurence of a critical wavelength corresponds to a neutrally stable transverse mode which leaves the system energy unchanged. We derive a stability criterion by determining under which conditions no critical wavelength can be found, that is, the conditions for which all transverse disturbances lead to an increase of the energy of the system. We find that stability is guaranteed if, for given substrate geometry and given contact angle, the unperturbed meniscus pressure is an increasing function of the liquid cross-sectional area.

The mathematical technique used here has been employed by others, for example Concus & Karasalo (1978), Karasalo (1979), Brown and Scriven (1980), Myshkis *et al.* (1987), and Sekimoto, Oguma & Kawazaki (1987). Another more prevalent technique in meniscus stability analysis is bifurcation theory: change in stability occurs whenever alternative bifurcating equilibrium solutions are present. The occurrence of a neutrally stable mode of perturbation corresponds to the joining of two or more branches of equilibrium solutions, here the branches of cylindrical interfaces and of three-dimensional wavy interfaces. We do not calculate here the new equilibrium interfaces which bifurcate from the cylindrical interfaces, as Brown & Scriven did for liquid menisci pinned to a slot.

Stability studies of cylindrical capillary surfaces can be found in the literature. Majumbar & Michael (1976) have examined the stability of two-dimensional pendant

drops formed in a channel of prescribed aperture, hanging from horizontal parallel edges at the same height. Hence the contact lines of the drop are pinned at two corner points, and the equilibrium is maintained by a balance of gravitational and surface tension forces. They examined the stability of the drop to both planar symmetric modes and to three-dimensional displacements having sinuous variation along the length of the drop. For apertures less than a critical value π times the capillary length $\sqrt{\sigma/\rho g}$ (where σ is the interfacial tension, ρ the liquid density and g the acceleration due to gravity), the drop pressure, as measured by the internal pressure at the aperture in excess of the external pressure, reaches a maximum as the volume and depth of the drop are gradually increased from zero. For drops maintained at constant volume within apertures less than π, they showed that instability will develop due to three-dimensional perturbations, whenever the two-dimensional equilibrium profile reaches a pressure maximum. Instability due to two-dimensional plane, symmetric, volume-conserving disturbances occurs when the volume of the suspended drop reaches a maximum value as a function of its depth. Since the pressure maximum occurs at a lower volume and a lower depth than the point of volume maximum, the drop will always become unstable to three-dimensional disturbances first. The limiting case of zero Bond number was analysed by Brown & Scriven (1980), and similar qualitative results were found.

Davis (1980) studied the stability of static rivulets partially wetting a flat surface, of height so small that gravitational effects are neglected. Here the contact lines of the equilibrium cylindrical liquid interface are allowed to move. Stability of the static meniscus is studied by a dynamic approach by linearization of the hydrodynamic equations which govern the small-amplitude disturbances of the rivulet. Three types of contact line conditions are considered: (i) fixed contact lines, (ii) moving contact lines with fixed contact angles, and (iii) contact angles which vary smoothly with contact-line speeds. The linearized equations of motion of each normal mode $\exp(\omega t + \mathrm{i}rkz)$ (where z is the coordinate along the axis of the cylindrical ridge of radius r) yield a energy balance equation of the form $E\omega^2 + \Phi\omega + I(k) = 0$ where E is the kinetic energy of small disturbances, Φ is the viscous dissipation, and I is the interfacial energy due to surface tension. A sufficient condition for stability is obtained in the form $I(k) > 0$ in all cases. In particular, for both cases (ii) and (iii) of contact line motion, the same stability condition is obtained by deriving a lower bound for $I(k)$. Setting this lower bound to zero yields an expression for the critical wavenumber k_c: all normal modes of wavenumber $0 < k < k_c$ are unstable. We will show that the necessary condition for stability found by Davis is a particular case of our results.

Our study is organized as follows: in § 2, we determine the first- and second-order variations of the system interfacial energy, and we obtain the equations governing the equilibrium capillary surface and the condition for stability as the positivity of a quadratic functional $Q(\eta)$; in § 3, we arrive at a stability criterion and the critical wavelength of instability by showing that the variational problem $\min Q > 0$ is equivalent to an eigenvalue problem governing the modes of instability; in § 4, we apply our stability analysis to a number of substrate configurations where we recover previously known results and show new results; finally, in § 5, we conclude with a few remarks and with possible generalizations.

2. First- and second-order variation of the energy

We consider whether equilibrium capillary surfaces which partially wet a solid substrate are stable to transverse perturbations. We neglect the influence of gravity,

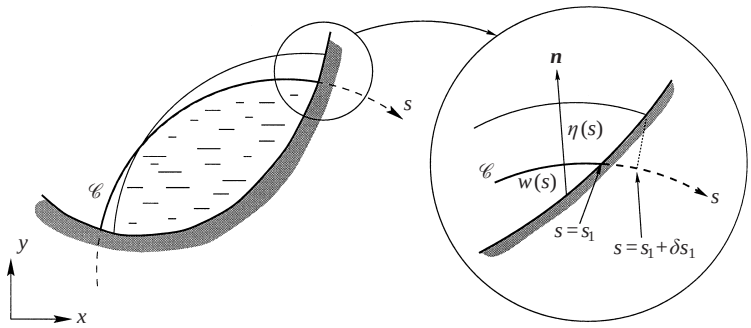

FIGURE 1. Cross-section of cylindrical liquid ridge through a plane z = constant.

since the Bond number $Bo = \rho g L^2/\sigma$ is assumed small compared to unity. The liquid interface is surrounded by a passive gas of constant atmospheric pressure which may be taken to be zero without loss of generality. The unperturbed liquid configuration and the substrate shape are independent of the coordinate z of a Cartesian coordinate system ($Oxyz$). See figure 1. We assume that both surfaces are infinite cylinders with generatrices parallel to the z-axis. The unperturbed liquid–vapour interface $\mathscr{S}$ may be described by the equations

$$x = X(s), \quad y = Y(s), \quad s_0 \leqslant s \leqslant s_1, \tag{2.1}$$

where s is the arclength measured along the curve of intersection $\mathscr{C}$ between the liquid-vapour interface and any plane $z =$ constant. The unperturbed contact lines are the straight lines $s = s_0$ and $s = s_1$ where the three interfaces solid–vapour, solid–liquid and liquid–vapour intersect. We assume that the liquid is to the right of $\mathscr{C}$ as one moves on $\mathscr{C}$ in the direction of increasing s. Then the mean curvature (defined herein as the sum of the principal curvatures) of the interface is given by

$$\kappa(s) = X'(s)Y''(s) - Y'(s)X''(s), \tag{2.2}$$

where primes denote derivatives with respect to the variable s. We consider the class of infinitesimal, smooth perturbations formed by displacing each point (s, z) of $\mathscr{S}$ a small distance $\eta(s, z)$ in the direction of the outward normal $\boldsymbol{n}$ at that point. Hence we obtain the following representation:

$$x = X(s) - \eta(s, z)Y'(s), \quad y = Y(s) + \eta(s, z)X'(s), \quad z = z, \tag{2.3}$$

where $s_0 + \delta s_0 \leqslant s \leqslant s_1 + \delta s_1$. The cylindrical solid interface may be parametrized by the arclength s in the following way

$$x = X(s) - w(s)Y'(s), \quad y = Y(s) + w(s)X'(s), \tag{2.4}$$

over a neighbourhood of the unperturbed contact lines $s = s_0$ and $s = s_1$, and where $w(s)$ represent the coordinate of a point of the wall measured on the normal $\boldsymbol{n}$ at a point of $\mathscr{C}$. See figure 1. Since normals to the liquid free surface may intersect, representation (2.4) is only valid over sufficiently small sections of substrate. This representation is in fact only needed in a small neighbourhood of the contact lines. See additional remarks in Appendix A. The intersection of the solid and liquid interfaces at the contact lines imposes the condition

$$w(s_i) = 0 \tag{2.5}$$

for the unperturbed state, and

$$\delta s_i(z) = \frac{\eta(s_i, z)}{w'(s_i)} \tag{2.6}$$

for the perturbed state, within first-order of perturbation δs_i and $\eta(s_i)$.

The liquid interface is in equilibrium if the total energy $\mathscr{E} = \sigma \mathscr{A}_{LV} + \sigma_{SV}\mathscr{A}_{SV} + \sigma_{SL}\mathscr{A}_{SL}$ associated with the surface forces acting at all interfaces reaches a stationary value. Here $\mathscr{A}_{LV}$, $\mathscr{A}_{SV}$ and $\mathscr{A}_{SL}$ are the areas of the liquid-vapour, solid-vapour, and solid-liquid interfaces, respectively, with corresponding surface energies σ, σ_{SV}, and σ_{SL}. This can be expressed by stating that the variation $\delta\mathscr{E}$ of the system's energy is zero for all infinitesimal perturbations η which leave the volume V of the liquid domain unchanged. We note at this point that this variational isoperimetric problem should be solved more rigorously by using a two-parameter family $\epsilon_1\eta_1 + \epsilon_2\eta_2$ of comparison functions (perturbations) in order to properly guarantee the volume constraint. We show in Appendix B that a one-parameter family is in fact sufficient.

Our constrained optimization problem can be written as the variation

$$\delta\mathscr{E}(\eta) + \mu\delta V(\eta) = \sigma\delta\mathscr{A}_{LV} + (\sigma_{SL} - \sigma_{SV})\delta\mathscr{A}_{SL} + \mu\,\delta V = 0, \tag{2.7}$$

where μ is a Lagrange multiplier, and where we have used $\delta\mathscr{A}_{SV} = -\delta\mathscr{A}_{SL}$ for the variation of area of the solid-vapour interface. With the adopted parametrization, and over a length λ along the z-axis, we find (see Appendix A for details)

$$\begin{aligned}\delta\mathscr{E}(\eta) + \mu\delta V(\eta) = &\int_0^\lambda \int_{s_0+\delta s_0}^{s_1+\delta s_1} \{\sigma f_A(\eta, \eta_s, \eta_z) - \sigma + \mu f_V(\eta)\}\,\mathrm{d}s\,\mathrm{d}z \\ &+ \int_0^\lambda \int_{s_0+\delta s_0}^{s_0} \{\sigma + (\sigma_{SL} - \sigma_{SV})\, f_A(w, w', 0) - \mu f_V(w)\}\,\mathrm{d}s\,\mathrm{d}z \\ &+ \int_0^\lambda \int_{s_1}^{s_1+\delta s_1} \{\sigma + (\sigma_{SL} - \sigma_{SV})\, f_A(w, w', 0) - \mu f_V(w)\}\,\mathrm{d}s\,\mathrm{d}z,\end{aligned} \tag{2.8}$$

where the functions f_A and f_V are given by

$$f_A(\eta, \eta_s, \eta_z) = \left\{(1 - \kappa(s)\eta)^2(1 + \eta_z^2) + \eta_s^2\right\}^{1/2}, \quad f_V(\eta) = \eta(1 - \tfrac{1}{2}\kappa(s)\eta), \tag{2.9}$$

with $\eta_s = \partial\eta/\partial s$, $\eta_z = \partial\eta/\partial z$. We then expand $\delta\mathscr{E} + \mu\delta V$ to first order by linearization with respect to the small variations η and δs_i to find

$$\begin{aligned}\delta\mathscr{E} + \mu\delta V = &\int_0^\lambda \int_{s_0}^{s_1} \left\{\sigma\left(\frac{\partial f_A}{\partial \eta}\right)_0 \eta + \sigma\left(\frac{\partial f_A}{\partial \eta_s}\right)_0 \eta_s + \sigma\left(\frac{\partial f_A}{\partial \eta_z}\right)_0 \eta_z + \mu\left(\frac{\partial f_V}{\partial \eta}\right)_0 \eta\right\} \mathrm{d}s\,\mathrm{d}z \\ &+ \sum_{i=0}^{1} (-1)^{i+1} \int_0^\lambda (\sigma + (\sigma_{SL} - \sigma_{SV})\, f_A(w, w', 0) - \mu f_V(w))_{s=s_i} \delta s_i(z)\mathrm{d}z = 0,\end{aligned}$$

where the partial derivatives of f_A and f_V are taken at $(\eta, \eta_s, \eta_z) = (0, 0, 0)$:

$$\left(\frac{\partial f_A}{\partial \eta}\right)_0 = -\kappa(s), \quad \left(\frac{\partial f_A}{\partial \eta_s}\right)_0 = 0, \quad \left(\frac{\partial f_A}{\partial \eta_z}\right)_0 = 0, \quad \left(\frac{\partial f_V}{\partial \eta}\right)_0 = 1.$$

The stationarity condition leads to the well-known Laplace equation statisfied by the equilibrium surface $\mathscr{S}$:

$$-\sigma\kappa(s) + \mu = 0, \quad s_0 \leqslant s \leqslant s_1, \tag{2.10}$$

and to the Young–Laplace condition at the contact lines

$$\sigma + (\sigma_{SL} - \sigma_{SV})\, f_A(w(s_i), w'(s_i), 0) - \mu f_V(w(s_i)) = 0, \quad i = 0, 1. \tag{2.11}$$

Equation (2.10) shows that the mean curvature $\kappa(s)$ is a constant, and as expected, the equilibrium cross-sectional curve $\mathscr{C}$ is an arc of circle of radius $r = \pm 1/\kappa$. In the derivations which follow, we treat κ as a constant parameter and replace the Lagrange multiplier μ by $\sigma\kappa$. We call a meniscus 'concave' if $\kappa > 0$, and conversely 'convex' if $\kappa < 0$ (as shown in figure 1). Equation (2.11) can be written as, using $w(s_i) = 0$, $i = 0, 1$,

$$\frac{\sigma_{SV} - \sigma_{SL}}{\sigma} = (1 + w'(s_i)^2)^{-1/2} = \boldsymbol{n} \cdot \boldsymbol{n}_w \equiv \cos\gamma, \quad i = 0, 1, \tag{2.12}$$

where γ, the so-called *contact angle*, is the angle measured between the two outward unit normal vectors $\boldsymbol{n}$ and $\boldsymbol{n}_w$ of the liquid interface and solid wall at the contact lines. Hence it follows that

$$w'(s_i) = (-1)^{i+1} \tan\gamma, \quad i = 0, 1. \tag{2.13}$$

With these conditions assumed to hold, the equilibrium surface $\mathscr{S}$ is stable if the energy variation $\delta\mathscr{E}(\eta)$ remains positive for all second-order perturbations in the neighbourhood of $\mathscr{S}$, for all η such that $\delta V(\eta) = 0$. Hence we determine $\delta\mathscr{E}(\eta) + \mu\delta V(\eta)$ within quadratic terms in the perturbations η and δs_i (see Appendix A):

$$\frac{1}{2\sigma}(\delta\mathscr{E} + \mu\delta V) = \int_0^{\lambda}\int_{s_0}^{s_1} \{\eta_s^2 + \eta_z^2 - \kappa^2\eta^2\}\, \mathrm{d}s\, \mathrm{d}z + \sum_{i=0}^{1}(-1)^i \int_0^{\lambda} \frac{\mathrm{d}}{\mathrm{d}s}\{\cos\gamma\, f_A(w, w', 0) + \kappa f_V(w)\}_{s=s_i} \delta s_i^2(z)\mathrm{d}z, \tag{2.14}$$

where we have used the identities $\mu = \sigma\kappa$ and $\sigma_{SV} - \sigma_{SL} = \sigma\cos\gamma$. Upon using the contact line conditions $w(s_i) = 0$, $w'(s_i) = (-1)^{i+1}\tan\gamma$ and the relationship (2.6) between $\delta s_i(z)$ and $\eta(s_i, z)$, we find

$$\frac{1}{2\sigma}(\delta\mathscr{E} + \mu\delta V) = \int_0^{\lambda}\int_{s_0}^{s_1} \{\eta_s^2 + \eta_z^2 - \kappa^2\eta^2\}\, \mathrm{d}s\, \mathrm{d}z + \int_0^{\lambda} \{\alpha_0\eta^2(s_0, z) + \alpha_1\eta^2(s_1, z)\}\, \mathrm{d}z, \tag{2.15}$$

with

$$\alpha_i = -\cot\gamma\,(\kappa\sin^2\gamma + w''(s_i)\cos^2\gamma), \quad i = 0, 1. \tag{2.16}$$

The second derivative of w at the contact lines is of course related to the curvature $\kappa_w(s_i)$ at the contact lines of the cross-section of the solid interface with a plane $z =$ constant. It can readily be shown that

$$\kappa_w(s_i) = \cos^3\gamma\, \left(w''(s_i) + \kappa + 2\kappa\tan^2\gamma\right)$$

which leads to

$$\alpha_i = \frac{\kappa\cos\gamma - \kappa_w(s_i)}{\sin\gamma}, \quad i = 0, 1, \tag{2.17}$$

where we choose the sign of κ_w so that $\kappa_w > 0$ when the curvature vector of the solid surface is directed along the outward normal $\boldsymbol{n}_w$. Hence the stability of equilibrium surface $\mathscr{S}$ can be guaranteed if the minimum value reached by the functional

$$Q(\eta) = \frac{1}{2}\int_0^{\lambda}\int_{s_0}^{s_1} \{\eta_s^2 + \eta_z^2 - \kappa^2\eta^2\}\, \mathrm{d}s\, \mathrm{d}z + \frac{1}{2}\int_0^{\lambda} \{\alpha_0\eta^2(s_0, z) + \alpha_1\eta^2(s_1, z)\}\, \mathrm{d}z \tag{2.18}$$

over the set of smooth functions $\eta(s,z)$ satisfying the condition

$$\int_0^{\lambda}\int_{s_0}^{s_1}\eta(s,z)\mathrm{d}s\,\mathrm{d}z=0 \tag{2.19}$$

is a positive number.

3. Stability criterion

Variational problems such as $Q(\eta)=\min$ constrained by equation (2.19) are known to be related to the eigenvalue problem associated with a linear operator (see Courant & Hilbert 1953, vol I, Chapter VI). Indeed, if in addition to the volume constraint (2.19) we require that the set of admissible functions η also satisfy the normalization constraint

$$\int_0^{\lambda}\int_{s_0}^{s_1}\eta^2(s,z)\mathrm{d}s\,\mathrm{d}z=1 \tag{3.1}$$

then this variational problem leads to the Euler–Lagrange equation (see Appendix C)

$$\eta_{ss}+\eta_{zz}+\kappa^2\eta+\mu_0+\mu\eta=0, \tag{3.2}$$

where μ_0 and μ are the Lagrange multipliers associated with the constraints (2.19) and (3.1), with the following boundary conditions:

$$\eta_s(s_1,z)+\alpha_1\eta(s_1,z)=-\eta_s(s_0,z)+\alpha_0\eta(s_0,z)=0, \tag{3.3}$$

$$\eta_z=0,\quad z=0,\ \lambda. \tag{3.4}$$

Furthermore, we show in Appendix C that the minimum value reached by $Q(\eta)$ is the smallest eigenvalue $\min(\mu)$ solution of equation (3.2) with boundary conditions (3.3)–(3.4). Note that the normalization condition (3.1) can be imposed without loss of generality since it does not affect in any way the requirement that the quadratic functional Q remain positive. The stability criterion of $\mathscr{S}$ now becomes $\min(\mu)>0$.

The solution of (3.2)–(3.4) can be found by expanding the unknown eigenfunction in the expansion

$$\eta(s,z)=\eta_0(s)+\sum_{n=1}^{\infty}\eta_n(s)\cos\left(\frac{n\pi z}{\lambda}\right). \tag{3.5}$$

Then the modes η_0 are solutions of

$$\eta_0''+\kappa^2\eta_0+\mu_0+\mu\eta_0=0,\quad s_0\leqslant s\leqslant s_1,\quad \int_{s_0}^{s_1}\eta_0(s)\mathrm{d}s=0, \tag{3.6}$$

$$\eta_0'(s_1)+\alpha_1\eta_0(s_1)=-\eta_0'(s_0)+\alpha_0\eta_0(s_0)=0, \tag{3.7}$$

and correspond to perturbations in the (Oxy)-plane. The modes η_n, $n\geqslant 1$, automatically satisfy the volume constraint (2.19) and are the non-trivial solutions of

$$\eta_n''+\left(\mu+\kappa^2-\left(\frac{n\pi}{\lambda}\right)^2\right)\eta_n=0,\quad s_0\leqslant s\leqslant s_1, \tag{3.8}$$

$$\eta_n'(s_1)+\alpha_1\eta_n(s_1)=-\eta_n'(s_0)+\alpha_0\eta_n(s_0)=0, \tag{3.9}$$

and correspond to transverse periodic perturbations of wavelength 2λ.

We note at this point that the modes of perturbations we have found are strictly valid for a liquid ridge of finite length λ, that is, for liquid domains bounded by flat

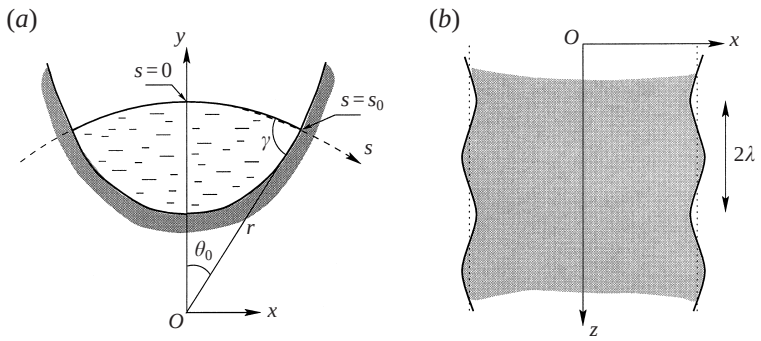

FIGURE 2. (*a*) Symmetrical liquid ridge with centreplane $x = 0$. (*b*) Transverse varicose-like mode of instability of wavelength 2λ of a meniscus with free contact lines.

surfaces at $z = 0$ and $z = \lambda$ with contact angle $\pi/2$ (to ensure a cylindrical interface). The question is then to find, for given substrate and cross-sectional liquid geometries, the critical length λ_c above which a liquid cylindrical ridge becomes unstable.

Since this analysis is valid for arbitrarily large ridge length, we adopt the viewpoint that, for an infinitely long ridge, the relevant modes of perturbations are still of the type $\eta_0(s)$ (planar modes) and $\eta_n(s)\cos(\pi z/\lambda)$, i.e. transverse periodic modes of wavelength 2λ continuously ranging from 0 to ∞. The problem is then to determine the smallest wavelength $2\lambda_c$ above which all transverse periodic perturbations are destabilizing. Whether other types of perturbations are relevant is a mathematical question which is beyond the scope of this article. Hence, for infinite configurations, our analysis is valid strictly with respect to the aforementioned class of perturbations. In the following derivations and in the particular examples treated in § 4, the parameter $\lambda_c = \pi/k_c$ is to be interpreted either as the critical length of a finite ridge or as the *half-wavelength* of the critical mode of instability for an infinitely-long ridge.

We now determine the eigenmodes for symmetric configurations, that is, for which the contact line conditions at $s = s_0$ and $s = s_1$ are identical: $\alpha_0 = \alpha_1 = \alpha$. In particular, this would be satisfied if the solid interface admits a plane of symmetry $x = 0$ as shown in figure 2. Then for liquid menisci with the same symmetry, we may replace the boundary conditions satisfied by the modes η_n by conditions at $s = 0$ (on the plane of symmetry) and at $s = s_0$ (on the wall)

$$\eta_n'(0) = 0, \quad \eta_n'(s_0) + \alpha\eta_n(s_0) = 0 \quad (n \geqslant 0), \tag{3.10}$$

where $\alpha = (\kappa\cos\gamma - \kappa_w)/\sin\gamma$, and $r = \pm 1/\kappa$, θ_0 and $s_0 = r\theta_0$ now denote the radius, the half-angle, and the half-arclength, respectively, of the equilibrium meniscus (see figure 2). Then we find the following solutions, within an arbitrary non-zero multiplicative constant:

$$\eta_0(s) = \cos(s\sqrt{\kappa^2 + \mu}) - \frac{\sin(s_0\sqrt{\kappa^2 + \mu})}{s_0\sqrt{\kappa^2 + \mu}}, \tag{3.11}$$

where the constants $\mu \neq -1/r^2$ are the roots of the equation

$$(\xi + r\theta_0\alpha/\xi)\tan\xi = r\theta_0\alpha, \quad \xi = \theta_0\sqrt{1 + r^2\mu} \tag{3.12}$$

($\mu = -1/r^2$ must be discarded as a possible eigenvalue unless $\alpha = -3/s_0$). If the smallest root of this equation is positive, then the equilibrium surface $\mathscr{S}$ remains stable to planar modes (3.11).

For $n \geqslant 1$, the transverse modes take the expression

$$\eta_n(s) = \cos\left(s\sqrt{\kappa^2 + \mu_n - \left(\frac{n\pi}{\lambda}\right)^2}\right) \tag{3.13}$$

where the eigenvalues μ_n satisfy

$$\sqrt{\kappa^2 + \mu_n - \left(\frac{n\pi}{\lambda}\right)^2}\tan\left(s_0\sqrt{\kappa^2 + \mu_n - \left(\frac{n\pi}{\lambda}\right)^2}\right) = \alpha. \tag{3.14}$$

First, we note that the smallest eigenvalue μ_n is obtained for $n = 1$. Second, there exists a critical value of the half-wavelength λ for which $\min(\mu_1)$ is zero. This value corresponds to the critical value k_c of the wavenumber $k = \pi/\lambda$ for neutral stability of the liquid ridge. All wavenumbers $0 < k \leqslant k_c$ below k_c lead to sinuous (often coined 'varicose') modes of instability of the liquid ridge. If k_c exists, it must be a solution of the equation

$$\sqrt{1 - (rk_c)^2}\tan(\theta_0\sqrt{1 - (rk_c)^2}) = r\alpha \tag{3.15}$$

for $0 < rk_c < 1$, or

$$\sqrt{-1 + (rk_c)^2}\tanh(\theta_0\sqrt{-1 + (rk_c)^2}) = -r\alpha \tag{3.16}$$

for $rk_c > 1$. It is readily seen that equation (3.16) always admits a solution for $\alpha \leqslant 0$. However, for $\alpha > 0$, equation (3.15) will not admit a root satisfying $0 < rk_c < 1$ if the parameters α, θ_0 and γ satisfy the condition $r\alpha\cos\theta_0 - \sin\theta_0 > 0$:

$$(\kappa\cos\gamma - \kappa_w)\cos\theta_0 > \frac{1}{r}\sin\theta_0. \tag{3.17}$$

When the equality $r\alpha\cos\theta_0 = \sin\theta_0$ is satisfied, the critical wavenumber k_c is zero, that is, the wavelength of transverse instabilities becomes infinite. We show in Appendix D that the stability condition (3.17) is equivalent to

$$\left(\frac{\mathrm{d}p}{\mathrm{d}A}\right)_\gamma > 0, \tag{3.18}$$

where $p = -\sigma\kappa$ denotes the constant pressure within the cylindrical liquid meniscus, and where A is its cross-sectional area in a plane $z =$ constant. Here the pressure is viewed as a function of the liquid volume when the wall geometry and the contact angle γ remain fixed. This condition may be interpreted as follows: whenever $\mathrm{d}p/\mathrm{d}A > 0$, infinitesimal sinuous perturbations of very large wavelength lead to a pressure increase in the thicker sections, and hence will induce flow toward the thinner sections. The liquid ridge is then stable to infinite-wavelength transverse perturbations and hence to all perturbations.

The existence of a critical wavelength of instability depends on the specific dependence of the half-angle θ_0 and of the parameter α upon the geometry of the solid interface. We consider below a number of substrate configurations for which the equations (3.15) and (3.16) are solved numerically. In each case we check whether (3.17) or (3.18) can be realized or not.

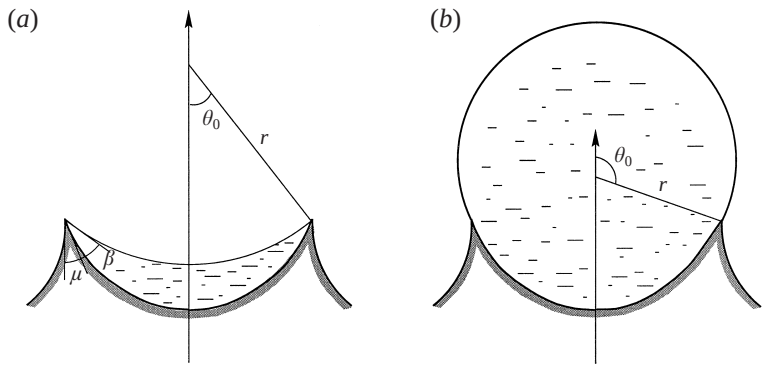

FIGURE 3. Cylindrical liquid ridge pinned to the two sharp edges of a groove. The dihedral angle β formed between the solid and liquid interfaces must satisfy $\gamma < \beta < \pi - \mu + \gamma$ to guarantee the existence of such a configuration. (*a*) $\theta_0 \leqslant \pi/2$, the liquid ridge is stable to all infinitesimal perturbations. (*b*) $\theta_0 > \pi/2$, the liquid ridge is unstable to all transverse sinuous perturbations of wavenumber $rk \leqslant rk_c = (1 - (\pi/2\theta_0)^2)^{1/2}$.

4. Applications

4.1. *Fixed contact lines*

Here we consider the case treated by Brown & Scriven (1980) of the stability of a liquid ridge whose contact lines are pinned at two symmetrically located locations on the substrate. This would occur if the liquid meniscus located within a slot (or groove) is pinned to the sharp, parallel edges of the slot. See figure 3. A liquid meniscus with pinned contact lines is physically realizable if it is energetically favoured relative to any neighbouring configurations with free contact lines. This requirement places bounds on the dihedral angle, denoted as β on figure 3(*a*), formed between the solid and liquid interfaces:

$$\gamma < \beta < \pi - \mu + \gamma, \tag{4.1}$$

where γ is the contact angle that would be reached on a smooth location of the substrate, and where $\mu < \pi$ is the internal dihedral angle formed between the solid interfaces at the sharp edge. For $\beta < \gamma$, the meniscus must recede into the interior of the groove, while for $\beta > \pi - \mu + \gamma$, the meniscus must run over the sharp edge of the groove.

Stability analysis can be obtained from our previous results by taking the formal limit $\alpha \to \infty$. We first see that, with respect to planar modes, equation (3.12) becomes, in the limit $\alpha \to \infty$, $\tan\xi = \xi$ whose smallest non-zero positive root is $\xi_0 \approx 4.49$ and hence leads to the smallest eigenvalue μ given by $r^2\mu = (\xi_0/\theta_0)^2 - 1$. Since the angle θ_0 is always less than π, the smallest eigenvalue μ is always positive. Therefore, menisci with fixed contact lines are always stable to planar volume-conserving perturbations. Second, with respect to transverse perturbations, equation (3.15) becomes in the limit $\alpha \to \infty$

$$rk_c = \sqrt{1 - \left(\frac{\pi}{2\theta_0}\right)^2} \tag{4.2}$$

as long as $\theta_0 \geqslant \pi/2$. Hence menisci satisfying $\theta_0 < \pi/2$ are stable to all transverse perturbations. Menisci satisfying $\theta_0 \geqslant \pi/2$ are unstable to all transverse perturbations of wavelength $2\lambda \geqslant 2\lambda_c = 2\pi/k_c$. Note that as $\theta_0 \to \pi/2$, $k_c \to 0$. Hence we recover the results of Brown & Scriven (1980). Figure 4 shows the interfacial pressure p/σ

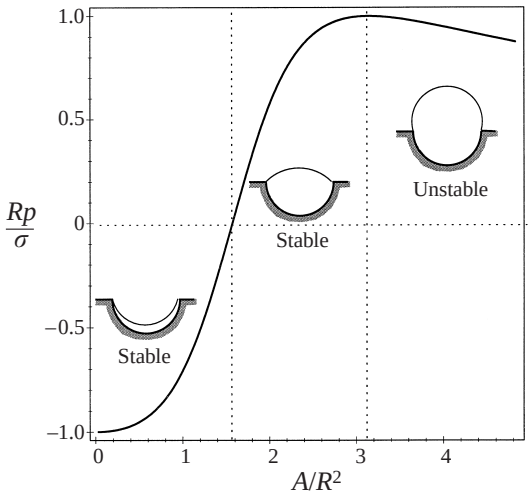

FIGURE 4. Cylindrical liquid ridge pinned to the two sharp edges of a semi-circular groove: interfacial pressure p/σ versus liquid ridge cross-sectional area A; the unstable menisci of half-angle $\theta_0 > \pi/2$ correspond to decreasing interfacial pressure, i.e. $\mathrm{d}p/\mathrm{d}A < 0$.

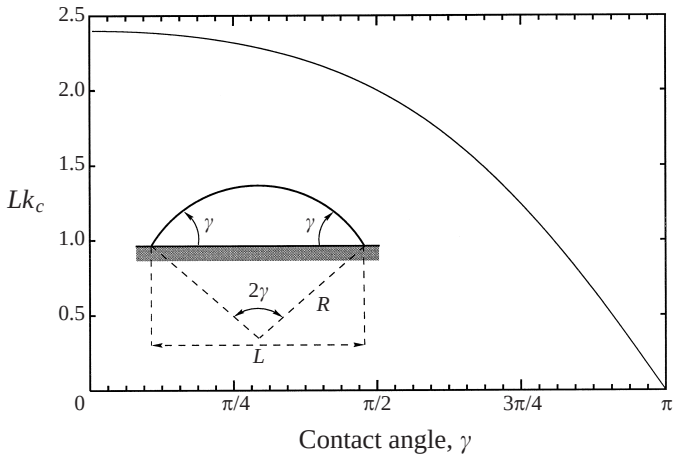

FIGURE 5. Critical wavenumber Lk_c for a flat surface versus the contact angle γ: (i) in the limit $\gamma \to 0$, $Lk_c \approx 2.40$, (ii) at $\gamma = \pi/2$, $Lk_c = 2$, (iii) in the limit $\gamma \to \pi$, $L \sim 2r(\pi - \gamma)$ leading to $rk_c = \text{constant} = \sqrt{3/4}$.

versus the cross-sectional liquid area $A \geqslant 0$ for the family of menisci pinned to the sharp edges of a semi-circular groove. It is seen that instability develops due to three-dimensional transverse perturbations when the two-dimensional equilibrium profile reaches a pressure maximum: stable menisci correspond to $\mathrm{d}\rho/\mathrm{d}A > 0$, while unstable menisci correspond to $\mathrm{d}p/\mathrm{d}A < 0$. The same criterion was found by Majumbar & Michael (1976) for pendant cylindrical menisci hanging from the edges of a slot.

4.2. *Planar substrate*

Here we generalize a result obtained by Sekimoto *et al.* (1987) in the case of a flat planar solid substrate. See figure 5. We readily obtain the angle θ_0 and the parameter

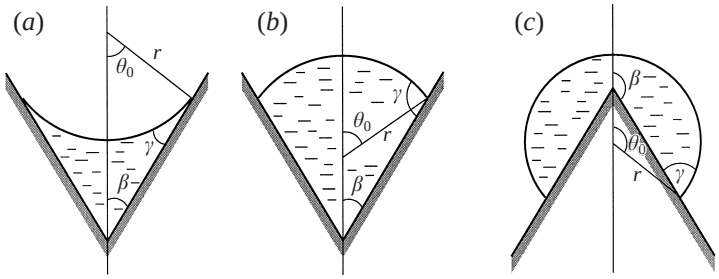

FIGURE 6. Liquid ridge wetting a wedge/edge: (*a*) concave meniscus (negative pressure) in a wedge, (*b*) convex meniscus (positive pressure) in a wedge, (*c*) convex meniscus wetting an edge of half-angle $\pi/2 < \beta < \pi$.

α for this geometry:

$$\theta_0 = \gamma, \quad \alpha = -\frac{1}{r}\cot\gamma. \tag{4.3}$$

First, we check that condition (3.17) can never be satisfied for $0 \leqslant \gamma \leqslant \pi$. It is also readily seen that, for given contact angle, the pressure within the cylindrical meniscus is a decreasing function of the liquid cross-sectional area, $\mathrm{d}p/\mathrm{d}A < 0$. We obtain three limiting cases of interest: (i) in the limit $\gamma \to 0$, we arrive at Sekimoto *et al.*'s result by scaling k_c with the distance $L = 2r\sin\gamma$ measured between the two contact lines, since in this range the radius of curvature r is of order $1/\gamma$. We then find that k_c satisfies $(Lk_c/2)\tanh(Lk_c/2) = 1$ yielding $Lk_c \approx 2.40$ independent of the value of the contact angle; (ii) for $\gamma = \pi/2$, the critical wavenumber should be identical to that of a liquid cylinder, that is, $rk_c = 1$ which is indeed the solution of (3.16); (iii) finally, in the limit $\gamma \to \pi$, we obtain a liquid cylinder pinned at one of its generatrices on the flat solid surface, and for which it is known that $rk_c \to \sqrt{3/4}$ which is indeed the solution of (3.15). Furthermore, we can check that, as expected, equation (3.12) has no negative roots $\mu \neq -1/r^2$, and hence the ridge is stable to planar modes. We solve the algebraic equations (3.15) and (3.16) by scaling k_c with the inverse of width L, and the results are shown in figure 5 for the entire range $0 \leqslant \gamma \leqslant \pi$. We believe that the same curve $k_c(\gamma)$ is found in the dynamic stability analysis done by Davis (1980) of static rivulets in contact with a flat substrate in the case of moving contact lines. It is not surprising that the critical wavenumber k_c should be independent of the dynamic modelization of contact lines. A dynamic modelization would however predict the growth rates of instability and the most unstable wavelength.

We note that the case of a liquid ridge of finite length λ at contact angle $\gamma = \pi/2$ is identical, by symmetry, to the case of a cylindrical liquid bridge between two parallel planes separated by a distance λ: we find that the critical length is $\lambda_c = \pi r$ which, as expected, is half of Rayleigh's wavelength of instability. For more details on the stability analysis of cylindrical bridges between flat surfaces, see Vogel (1987).

4.3. *Wedge and edge*

A natural extension of plane substrate is that of the wedge configuration shown in figure 6(*a*, *b*). The stability of menisci in wedge-like containers has been previously examined by Concus & Finn (1969, 1974) and more recently by Langbein (1990). We denote by β, $0 < \beta \leqslant \pi/2$, the half-angle of the wedge. We first note that non-symmetric menisci are not physically realizable if the contact angles of both walls of the wedge are identical. Two possible configurations of symmetric liquid ridges are

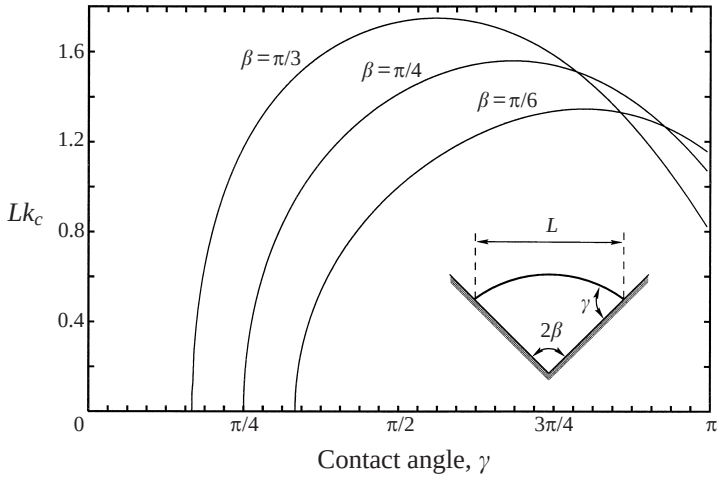

FIGURE 7. Non-dimensional critical wavenumber Lk_c for transverse instability of a meniscus of width L inside a wedge of angle 2β for $\beta = \pi/6, \pi/4, \pi/3$. For given fixed value of angle β, the menisci are stable to all modes of perturbation for contact angles $0 < \gamma \leqslant \pi/2 - \beta$ corresponding to concave (negative pressure) menisci.

possible. For a concave interface, that is, for a negative-pressure meniscus as shown in figure 6(*a*), we find

$$\theta_0 = \frac{\pi}{2} - \beta - \gamma, \quad \alpha = \frac{1}{r}\cot\gamma, \tag{4.4}$$

as long as the contact angle satisfies $0 \leqslant \gamma \leqslant \pi/2 - \beta$. Then it can be shown that condition (3.17) is always satisfied, and hence equations (3.15) and (3.16) do not admit any real roots. In the limit $\gamma \to \pi/2 - \beta$, the liquid surface becomes flat. Then, in this limit, $\theta_0 \to 0$ and $r = O(1/\theta_0)$ leading to $Lk_c \to 0$, if L denotes the distance between the two contact lines. Hence, for a contact angle $0 \leqslant \gamma \leqslant \pi/2 - \beta$, the liquid ridge is stable to all modes of perturbations (including planar modes, since (3.12) has no negative roots as expected).

For a convex interface, that is, for a positive-pressure meniscus as shown in figure 6(*b*), we find

$$\theta_0 = \beta + \gamma - \frac{\pi}{2}, \quad \alpha = -\frac{1}{r}\cot\gamma, \tag{4.5}$$

for a contact angle $\pi/2 - \beta \leqslant \gamma \leqslant \pi$. Then, condition (3.17) is never satisfied, and equations (3.15) and (3.16) always admit a root (Lk_c), with $Lk_c \to 0$ in the limit $\gamma \to \pi/2 - \beta$. Figure 7 shows (Lk_c) versus γ obtained by numerical solution of (3.15) and (3.16) for various wedge angles. We note that menisci in wedges are always stable in the limit of zero contact angle for all wedge angles $0 < \beta < \pi/2$.

For wedges of half-angle $\pi/2 < \beta < \pi$, or more appropriately termed 'edges', as shown in figure 6(*c*), the liquid interface is always convex, the parameters θ_0 and α are still given by (4.5), but the contact angle satisfies the bounds

$$\beta - \frac{\pi}{2} \leqslant \gamma \leqslant \frac{3\pi}{2} - \beta. \tag{4.6}$$

In the limit $\gamma \to 3\pi/2 - \beta$, the angle θ_0 tends to π, and the width L tends to 0: the cylindrical ridge is pinned at the edge vertex. In the limit $\gamma \to \beta - \pi/2$, the midpoint of the liquid interface comes into contact with the edge vertex.

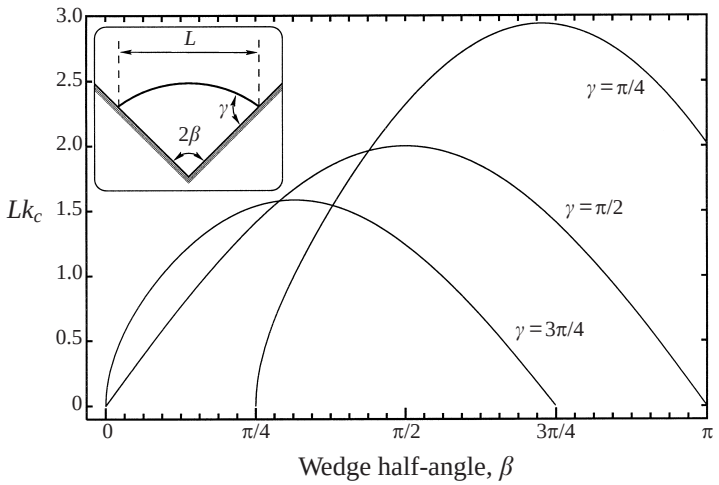

FIGURE 8. Non-dimensional critical wavenumber Lk_c for transverse instability of a meniscus inside a wedge of varying angle $0 \leqslant \beta \leqslant \pi$ and contact angle $\gamma = \pi/4, \pi/2, 3\pi/4$.

In figure 8, we show the variation of Lk_c as the wedge is 'opened' from the value $\beta = 0$ to $\beta = \pi$. In general, critical wavenumbers exist in the range

$$\beta_{min} = \max(0, \pi/2 - \gamma) \leqslant \beta \leqslant \beta_{max} = \min(\pi, 3\pi/2 - \gamma).$$

For all angles $0 < \beta \leqslant \beta_{min}$, the liquid ridge is stable for all perturbations. For $\beta_{max} \leqslant \beta < \pi$, the liquid ridge cannot exist as a whole but is divided into two symmetrical parts pinned at the edge vertex.

4.4. *Right-circular cylindrical solid surface*

We consider here the stability of liquid ridges partially wetting the interior surface of a cylinder of radius R. We fix the contact angle to some value γ between 0 and π. We build a family of liquid interfaces by increasing the liquid volume from 0 at some arbitrary point P of the solid surface until the entire interior of the cylinder is filled. We denote by A the ratio between the liquid area to the area of the vessel interior. As the fill ratio grows from $A = 0$, the menisci have positive decreasing pressure until the fill ratio $A_* = (2\gamma - \sin 2\gamma)/2\pi$ is reached. At $A = A_*$, the interface is straight and the pressure is zero. For increasing A from the value $A = A_*$ to $A = 1$, the menisci change convexity and have negative decreasing pressure. See figure 9. For each case, one can easily determine the parameters r, α, and θ_0 as a function of the fill ratio A and the contact angle γ. We find, for $0 < A < A_*$, denoting $\rho = r/R$,

$$A = \frac{1}{2\pi}(1 + \rho^2)(2\theta_0 - \sin 2\theta_0), \quad \cot\theta_0 = \frac{\rho + \cos\gamma}{\sin\gamma}, \quad r\alpha = -\frac{1}{\rho}\cot\theta_0, \tag{4.7}$$

and for $A_* < A < 1$

$$A = \frac{1}{2\pi}(1 - \rho^2)(2\theta_0 - \sin 2\theta_0), \quad \cot\theta_0 = \frac{\rho - \cos\gamma}{\sin\gamma}, \quad r\alpha = -\frac{1}{\rho}\cot\theta_0. \tag{4.8}$$

In both cases, condition (3.17) is never satisfied, and the equations (3.15) and (3.16) always admit a root (Lk_c), where we denote as before $L = 2r\sin\theta_0$ the distance between the contact lines. We obtain on figure 10 the various curves of $(Lk_c)_{A,\gamma}$ as functions of the fill ratio $0 \leqslant A \leqslant 1$ for fixed values of the contact angle in the

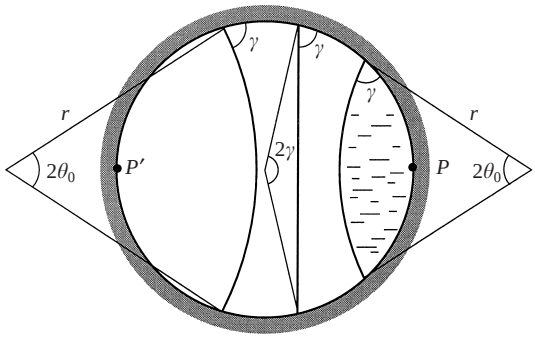

FIGURE 9. Liquid ridge wetting the interior of right-circular cylinder: as the fill ratio is increased from $A = 0$ at point P to $A = 1$ at point P', the menisci, initially convex (with positive pressure), become concave (with negative pressure).

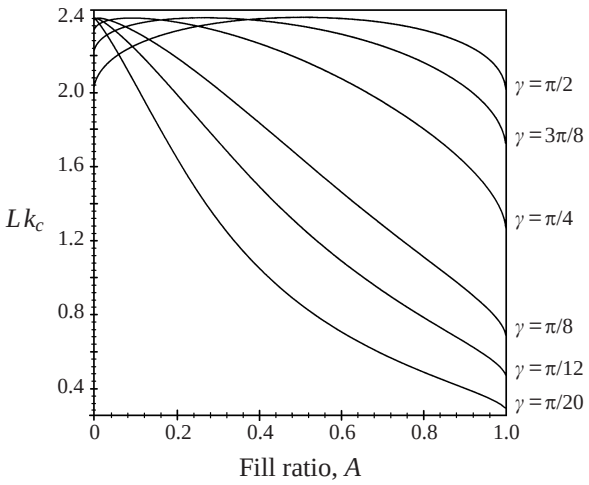

FIGURE 10. Critical wavenumber Lk_c versus fill ratio A for transverse instability of menisci partially wetting a right-circular cylinder for contact angle $\gamma = \pi/20$, $\pi/12$, $\pi/8$, $\pi/4$, $3\pi/8$, $\pi/2$. Note that for small contact angles and small fill ratio, the limit $Lk_c \approx 2.4$ is approached of a liquid ridge on a flat substrate at small contact angle.

interval $0 < \gamma \leqslant \pi/2$. Note that at $A \to 0$ or $A \to 1$, the width L tends to zero, and since Lk_c tends to a finite limit, the critical wavelength must tend to zero. As both A and γ tend to zero, we should expect to obtain the limit corresponding to a meniscus wetting a flat solid surface at small contact angle, that is, $Lk_c \to 2.40$. The corresponding curves for contact angle $\pi/2 < \gamma < \pi$ can be obtained from those shown in figure 10 by examination of figure 11: to a meniscus of contact angle γ and fill ratio A corresponds a 'complementary' one with contact angle $\pi - \gamma$ and fill ratio $1 - A$. Since both menisci admit the same values of the parameters r, θ_0, L and α, they must admit the same critical wavelength of instability according to equations (4.7) and (4.8):

$$(Lk_c)_{A,\gamma} = (Lk_c)_{1-A,\pi-\gamma}. \tag{4.9}$$

Hence the curves of figure 10 of contact angle $0 < \gamma < \pi/2$ will yield the corresponding ones for contact angle $\pi/2 < \gamma < \pi$ by symmetry about the line $A = 1/2$. Zero-contact-angle solutions are of course not possible, unless both contact lines coincide and lead

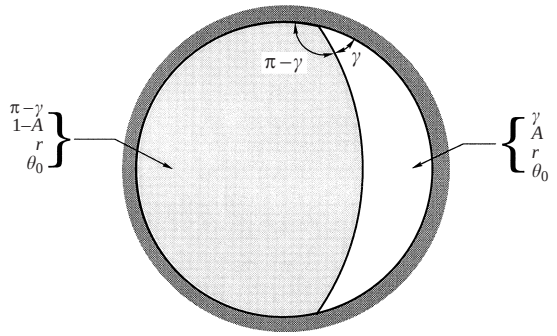

FIGURE 11. Two complementary menisci partially wetting a right-circular cylinder: if the meniscus to the right corresponds to fill ratio A and contact angle γ, then the meniscus to the left corresponds to fill ratio $1-A$ and contact angle $\pi-\gamma$; both menisci have the same critical wavelength of tranverse instability.

to right-circular cylindrical liquid interfaces with one generatrix pinned to the interior of the solid surface.

4.5. *Cylindrical solid surface of elliptical cross-section*

We can generalize the cylinder of circular cross-section to one with elliptical cross-section:

$$x = a\cos\phi, \quad y = b\sin\phi, \quad 0 \leqslant \phi < 2\pi, \tag{4.10}$$

where we choose $0 < c = b/a < 1$. We restrict our analysis to the family of menisci which are symmetric with respect to the plane $y = 0$, so that the contact line positions on the ellipse correspond to $\phi = \pm\phi_0$.† We denote again by r, θ_0, $(x_0, 0)$ the radius, the half-angle, and the coordinates of the centre of the arc of circle which represents the unperturbed meniscus. See figure 12(a). As in the previous case, a family of symmetric menisci of increasing volume can be generated by increasing the fill coefficient A from the value 0 at apex $P(a, 0)$ to the value 1 at apex $P'(-a, 0)$ for some given fixed value of the contact angle $0 \leqslant \gamma \leqslant \pi$. We find again that, at some fill ratio $A = A_*$, a straight liquid interface separates initially convex menisci from concave menisci. The contact line position of the straight meniscus on the ellipse is given as a function of γ by

$$\cos\phi_* = \frac{\cos\gamma}{\sqrt{\cos^2\gamma + c^2\sin^2\gamma}}, \tag{4.11}$$

with corresponding fill ratio given by

$$A_* = \frac{1}{\pi}(\phi_* - \tfrac{1}{2}\sin 2\phi_*). \tag{4.12}$$

Figure 12(b) shows a family of menisci generated from the apex P to apex P' for a contact angle $\gamma = 3\pi/8$ and $c = b/a = 1/2$. For fill ratio $0 < A < A_*$ and contact angle γ, the meniscus position is given by parameters $\rho = r/a$, $\xi = x_0/a$, ϕ_0, θ_0,

† There exists another less energetically favoured family of menisci which are symmetric with respect to the plane $x = 0$, with contact lines positions at $\phi = \phi_0$ and at $\phi = \pi - \phi_0$. We do not examine it. We note that a liquid layer lining the interior surface of a pipe with elliptical cross-section would have the tendency to flow towards the sharper 'corners' $P(a, 0)$ or $P'(-a, 0)$ due to gradients of substrate curvature.

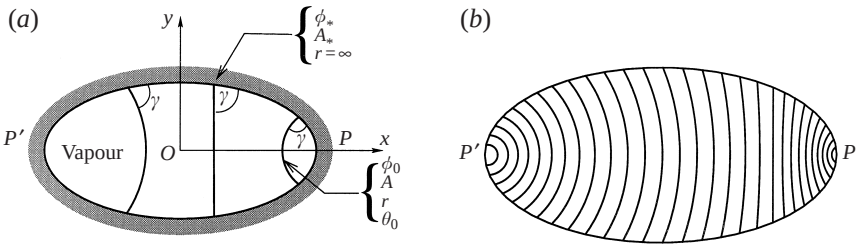

FIGURE 12. Menisci wetting the interior of a cylindrical surface with elliptical cross-section ($x = a\cos\phi, y = b\sin\phi$); (*a*) each meniscus is symmetric w.r.t plane $y = 0$ and is characterized by a fill ratio A, radius r, half-angle θ_0 and contact angle position ϕ_0 on the ellipse. The straight interface given by $\cos\phi_* = \cos\gamma/\sqrt{\cos^2\gamma + c^2\sin^2\gamma}$ separates convex from concave menisci. (*b*) A family of menisci of increasing volume generated from apex P (fill ratio $A = 0$) to apex P' (fill ratio $A = 1$) for $b/a = 1/2$ and contact angle $\gamma = 3\pi/8$. In (*a*) and (*b*) the liquid phase is assumed to the right of the vessel.

solutions of

$$\rho^2 = (\xi - \cos\phi_0)^2 + c^2\sin^2\phi_0, \quad \tan\theta_0 = \frac{c\sin\phi_0}{\xi - \cos\phi_0},$$
$$\rho = c\frac{-1 + \xi\cos\phi_0}{\cos\gamma\sqrt{\sin^2\phi_0 + c^2\cos^2\phi_0}}, \quad (4.13)$$

$$\pi A = \frac{\rho^2}{c}(2\theta_0 - \tfrac{1}{2}\sin 2\theta_0) + (\phi_0 - \tfrac{1}{2}\sin 2\phi_0). \quad (4.14)$$

The solutions of (3.15) and (3.16) can then be determined with the following expression for the parameter $r\alpha$:

$$r\alpha = -\frac{\cos\gamma + \rho\kappa_E}{\sin\gamma}, \quad \kappa_E = \frac{c}{(\sin^2\phi_0 + c^2\cos^2\phi_0)^{3/2}}, \quad (4.15)$$

where κ_E is the substrate curvature. Similar equations can be written for $A_* < A < 1$. The key difference between this case and the right-circular cylinder is that the equation $r\alpha\cos\theta_0 = \sin\theta_0$ may be satisfied only for some values of the fill ratio A for given contact angle γ. More specifically, for contact angles $0 \leqslant \gamma \leqslant \bar{\gamma}$, there exists a range of fill ratio $A_{min}(\gamma) \leqslant A \leqslant A_{max}(\gamma)$ for which condition (3.17) is satisfied; in this range, the liquid ridge is stable to transverse perturbations of all wavelengths. At $A = A_{max}$ or $A = A_{min}$, the wavelength is infinite. Note that at zero contact angle, the critical wavelength is given by

$$rk_c = \sqrt{1 - \left(\frac{\pi}{2\theta_0}\right)^2}, \quad \cos\theta_0 = \frac{c\cos\phi_0}{\sqrt{\sin^2\phi_0 + c^2\cos^2\phi_0}}, \quad \frac{\pi}{2} \leqslant \phi_0 \leqslant \pi. \quad (4.16)$$

Hence, all menisci which wet at most half of the ellipse perimeter at zero contact angle are stable to all perturbations: $A_{min} = 0$ and $A_{max} = (1-c)/2$ (since in the limit $\phi \to \pi/2$, $\rho \to c$, $\theta \to \pi/2$). Also note that in the limit $\phi \to \pi$ (i.e. when the contact lines approach P'), we have $\rho \to c^2$, $\theta \to \pi$ and $A \to 1 - c^3 < 1$ which corresponds to the circle osculating the ellipse at apex P'.

We show in figure 13 the numerical values reached by $(Lk_c)_{\gamma,A}$ in the range $0 \leqslant A \leqslant 1$, for a few contact angles in the interval $0 \leqslant \gamma \leqslant \pi/2$, and for the ratio $c = b/a = 0.5$: a range of stable menisci exists in the contact angle interval $0 \leqslant \gamma \leqslant \bar{\gamma} = 27^\circ\,3'$. Figure 14 delineates the regions of stability in the (γ, A) parameter

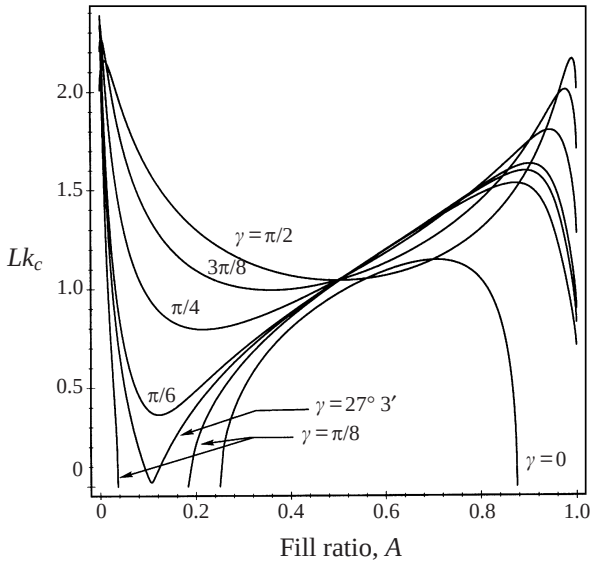

FIGURE 13. Critical wavelength of transverse instabilities for menisci partially wetting the interior of an elliptic cylinder. Each curve represents Lk_c versus the fill ratio $0 \leqslant A \leqslant 1$ for a specific contact angle $0 \leqslant \gamma \leqslant \pi/2$ and for $c = b/a = 1/2$. Similar curves can be graphed for $\pi/2 \leqslant \gamma \leqslant \pi$ by noting that $(Lk_c)_{A,\gamma} = (Lk_c)_{1-A,\pi-\gamma}$. Note that for $0 \leqslant \gamma \leqslant 27° 3'$, there is a range of menisci of fill ratio $A_{min} < A < A_{max}$ where k_c does not exist, i.e. for which the corresponding menisci are stable to sinuous transverse perturbations of all wavelengths. At zero contact angle, we have $A_{min} = 0$ and $A_{max} = 0.25$ which corresponds to menisci wetting at most half of the surface of the vessel.

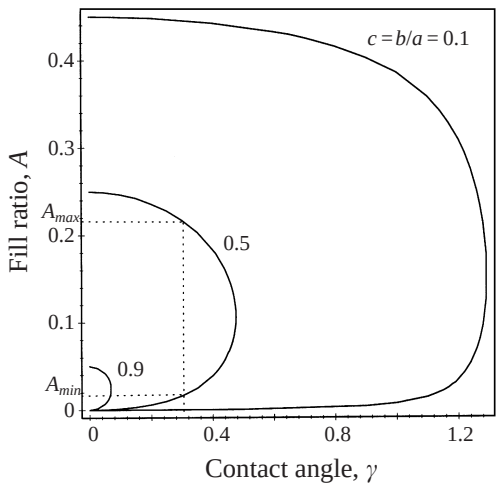

FIGURE 14. Fill ratio A_{min} and A_{max} versus contact angle γ for the ellipse geometry $c = b/a = 0.9, 0.5, 0.1$. In the range $A_{min} \leqslant A \leqslant A_{max}$, the menisci are stable to all transverse perturbations. As $c \to 1$, the range of stable menisci vanishes.

plane for the values $c = 0.1, 0.5, 0.9$. The region of stability decreases with the ellipse excentricity. Finally, figure 15 shows the variation of the meniscus pressure versus A for contact angle $\gamma = 0.3$ and $c = b/a = 0.5$, which clearly demonstrates that the range of stable menisci $A_{min} \leqslant A \leqslant A_{max}$ corresponds to $\mathrm{d}p/\mathrm{d}A > 0$.

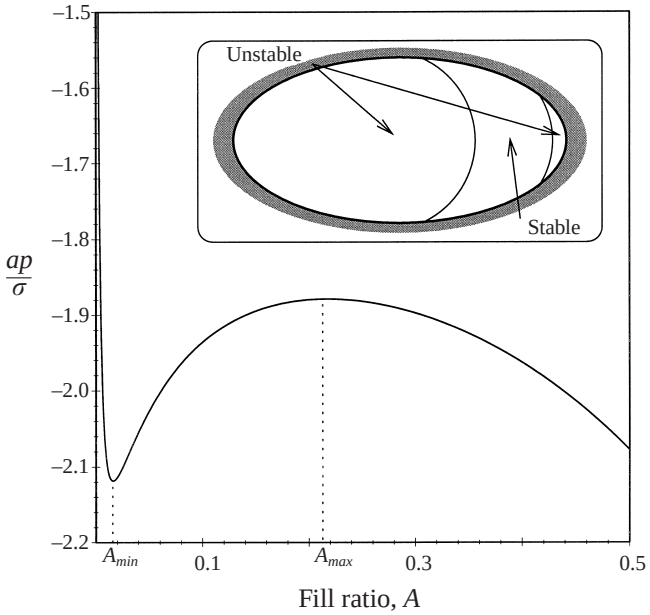

FIGURE 15. Pressure versus fill ratio for menisci partially wetting substrate of figure 12 for contact angle $\gamma = 0.3$ and $b/a = 0.5$: for fill ratio $A_{min} < A < A_{max}$, the menisci satisfy $\mathrm{d}p/\mathrm{d}A > 0$ and are stable to transverse perturbations. The inset shows the two critical menisci which separate stable and unstable solutions. These two interfaces are characterized by $\mathrm{d}p/\mathrm{d}A = 0$.

5. Concluding remarks

Our stability analysis of liquid ridges of finite length λ led to modes of instability of the type $\eta_n(s)\cos(n\pi z/\lambda)$, $n \geqslant 0$. For ridges of infinite length, we examined the stability with respect to the class of both planar and sinuous transverse modes of all wavelengths 2λ ranging from 0 to ∞ and we looked for the smallest possible wavelength (the critical wavelength) below which such perturbations are not destabilizing. When a certain inequality given by equation (3.17) is satisfied between the curvatures of the liquid and solid interfaces and the liquid–solid contact angle, no critical wavelength of instability can be found, and the resulting liquid ridge is stable with respect to this class of perturbations. Moreover, we found that this criterion is equivalent to the condition $\mathrm{d}p/\mathrm{d}A > 0$, which offers a practical way to assess the stability of a family of liquid ridges to transverse perturbations which conserve liquid volume. We believe that the same criterion would apply for other cylindrical configurations as for example in the case of liquid bridges between curved walls, or in the case of pendant liquid ridges. We note that an infinite cylindrical jet does not satisfy this condition, and hence is unstable, as predicted by Rayleigh. The question of whether other modes of perturbations are relevant to the stability analysis of infinite liquid ridges has not been addressed.

We have analysed the stability of liquid ridges to infinitesimal perturbations which preserve the liquid volume. Another class of perturbations are those which preserve the pressure difference across the interface, as would occur physically if the liquid ridge were connected to a constant-pressure reservoir. Such perturbations were considered by Majumbar & Michael (1977) and by Brown & Scriven (1980) for liquid menisci pinned to a slot.

Small deviations from the idealized case of zero Bond number are not expected to

qualitatively change the results presented here, as was shown in the studies of Brown & Scriven (at zero Bond number) and Majumbar & Michael (non-zero Bond number) for the stability of liquid menisci pinned to a slot. However, significant differences must be expected at large Bond numbers for pendant cylindrical menisci where the effect of gravitational forces leads to a maximum supportable volume of liquid.

Here we have determined the critical wavelength λ_c for instability; perturbation modes of greater wavelength are unstable. In a natural system excited by noise, an important quantity is the observed average wavelength at which a ridge of given cross-section on a given substrate will actually break up. Determination of this wavelength requires consideration of the fluid dynamics, including a model for flow and viscous dissipation at moving contact lines. It is necessary to relieve the so-called moving contact line singularity, i.e. the impossibility of contact-line motion for liquids with finite surface tension on a no-slip substrate (Huh & Scriven 1971). Significant progress can be made for the slow motion of thin liquid layers, when the lubrication approximation can be invoked. It is then possible to relieve the singularity through the use of a very thin 'precursor' layer applied on the nominally dry regions of the substrate. A finite equilibrium contact angle can also be incorporated in an efficient quasi-three-dimensional numerical model using a 'disjoining pressure' term in the resulting evolution equation (Schwartz 1998; Schwartz & Eley 1998). It should be noted, however, that this technique, like any other that treats moving contact lines, including various slip models, requires some degree of experimental validation. In the above-cited works, the precursor layer thickness is an adjustable parameter. Preliminary results show that the break-up of a slightly perturbed cylindrical ridge on a flat substrate can be modelled successfully for the entire period of motion, until the liquid finds a stable final configuration as a pattern of isolated drops. A report will be available shortly.

This work is supported by the NASA Microgravity Program, the ICI Strategic Research Fund, and the State of Delaware.

Appendix A. Derivation of the energy first and second variations

We define $\delta\mathscr{E} = \mathscr{E}(\eta) - \mathscr{E}(0)$ as the difference of interfacial energy between the perturbed and unperturbed configurations. With the parametrization (2.3), the surface admits the following metrics:

$$E \equiv \boldsymbol{x}_s^2 = (1-\kappa\eta)^2 + \eta_s^2, \quad F \equiv \boldsymbol{x}_s \cdot \boldsymbol{x}_z = \eta_s\eta_z, \quad G \equiv \boldsymbol{x}_z^2 = 1 + \eta_z^2, \tag{A 1}$$

where $\boldsymbol{x}(s,z)$ represents a position vector from the origin O to a point on the perturbed liquid interface. Hence its area can be expressed as (over a length λ along the z-axis)

$$\begin{aligned}\mathscr{A}_{LV}(\eta) &= \int_0^{\lambda}\int_{s_0+\delta s_0}^{s_1+\delta s_1} (EG-F^2)^{1/2}\mathrm{d}s\,\mathrm{d}z = \int_0^{\lambda}\int_{s_0+\delta s_0}^{s_1+\delta s_1} ((1-\kappa\eta)^2(1+\eta_z^2)+\eta_s^2)^{1/2}\mathrm{d}s\,\mathrm{d}z \\ &\equiv \int_0^{\lambda}\int_{s_0+\delta s_0}^{s_1+\delta s_1} f_A(\eta,\eta_s,\eta_z)\mathrm{d}s\,\mathrm{d}z. \end{aligned} \tag{A 2}$$

The liquid region confined between the solid and the liquid interfaces can be parametrized by (s,ξ,z) according to the (orthogonal) mapping

$$x = X(s) - \xi Y'(s), \quad y = Y(s) + \xi X'(s), \quad z = z, \tag{A 3}$$

with corresponding metrics

$$m_s = 1 - \kappa\xi, \quad m_\xi = 1, \quad m_z = 1. \tag{A 4}$$

Hence the volume of this region is

$$V(\eta) = \int_0^\lambda \int_{s_0+\delta s_0}^{s_1+\delta s_1} \int_{w(s)}^{\eta(s)} (1-\kappa\xi)\mathrm{d}\xi \mathrm{d}s\,\mathrm{d}z = \int_0^\lambda \int_{s_0+\delta s_0}^{s_1+\delta s_1} (f_V(\eta) - f_V(w))\mathrm{d}s\,\mathrm{d}z, \tag{A 5}$$

with $f_V(\eta) = \eta(1 - \frac{1}{2}\kappa\eta)$. Finally, the area of wetted wall is given by

$$\mathscr{A}_{SL}(\eta) = \int_0^\lambda \int_{s_0+\delta s_0}^{s_1+\delta s_1} f_A(w, w', 0)\mathrm{d}s\,\mathrm{d}z. \tag{A 6}$$

Then expression (2.8) is obtained by determining the variation of $\sigma\mathscr{A}_{LV} + \sigma_{SL}\mathscr{A}_{SL} + \sigma_{SV}\mathscr{A}_{SV} + \mu V$ between the unperturbed and perturbed configurations and by using $\delta\mathscr{A}_{SV} = -\delta\mathscr{A}_{SL}$. By expanding f_A and f_V in a Taylor series up to terms of first order in η, η_s and η_z, we find

$$\int_0^\lambda \int_{s_0+\delta s_0}^{s_1+\delta s_1} \{\sigma f_A(\eta, \eta_s, \eta_z) - \sigma + \mu f_V(\eta)\}\,\mathrm{d}s\,\mathrm{d}z \approx \int_0^\lambda \int_{s_0}^{s_1} (\mu - \sigma\kappa)\eta \mathrm{d}s\,\mathrm{d}z, \tag{A 7}$$

$$\int_0^\lambda \int_{s_i}^{s_i+\delta s_i} \{\sigma + (\sigma_{SL} - \sigma_{SV})\, f_A(w, w', 0) - \mu f_V(w)\}\,\mathrm{d}s/\mathrm{d}z$$
$$\approx \int_0^\lambda \left(\sigma + (\sigma_{SL} - \sigma_{SV})\, f_A(w, w', 0) - \mu f_V(w)\right)_{s=s_i} \delta s_i(z)\mathrm{d}z. \tag{A 8}$$

Since the perturbations η and δs_i are arbitrary, the equilibrium conditions (2.10) and (2.11) follow by imposing $\delta\mathscr{E} + \mu\delta V = 0$.

Assuming that conditions (2.10) and (2.11) are satisfied by the equilibrium meniscus, the second-order variation of $\mathscr{E} + \mu V$ is obtained by expansion to second-order terms in the perturbation η and δs_i:

$$\int_0^\lambda \int_{s_0+\delta s_0}^{s_1+\delta s_1} \{\sigma f_A(\eta, \eta_s, \eta_z) - \sigma + \mu f_V(\eta)\}\,\mathrm{d}s\,\mathrm{d}z \approx \frac{1}{2}\int_0^\lambda \int_{s_0}^{s_1} \left(\sigma\eta_s^2 + \sigma\eta_z^2 - \mu\kappa\eta^2\right)\mathrm{d}s\,\mathrm{d}z, \tag{A 9}$$

$$\int_0^\lambda \int_{s_i}^{s_i+\delta s_i} \{\sigma - \sigma\cos\gamma\, f_A(w, w', 0) - \mu f_V(w)\}\,\mathrm{d}s/\mathrm{d}z$$
$$\approx \frac{1}{2}\int_0^\lambda \frac{d}{ds}(\sigma - \sigma\cos\gamma\, f_A(w, w', 0) - \mu f_V(w))_{s=s_i} \delta s_i^2(z)\mathrm{d}z. \tag{A 10}$$

By using the contact line conditions for w and δs_i, one readily obtains the quadratic functional Q defined by (2.18).

Note that the representations (2.3) and (2.4) of the liquid and the solid surfaces in the vicinity of the contact lines lead to certain modifications for contact angle $\gamma \geqslant \pi/2$:

(i) The sign of $\mathscr{A}_{SL}$ should be reversed for $\gamma > \pi/2$; indeed, in this case the orientation of the solid surface in the vicinity of the contact lines according to (2.4) is reversed; this would then change the sign of $(1 + w'(s_i)^2)^{-1/2}$ in (2.12).

(ii) For $\gamma = \pi/2$, the relationship between $\eta(s_i)$ and δs_i needs to be appropriately modified since in this case $w'(s_i) \to \infty$. Moreover, a flat substrate is represented by the entire normal to the circular section at the contact line $s = s_i$. In this case, an arbitrary disturbance is still represented by (2.3) for $s_0 \leqslant s \leqslant s_1$ without the need to introduce the variations δs_i, or equations (2.5) and (2.6). The first and second variations would have to be rederived in this particular case. We find of course the same functional Q with $\alpha_0 = \alpha_1 = 0$.

Appendix B. Isoperimetric problems: one-parameter versus two-parameter comparison functions

We address here the validity of our solution procedure for variational problems of the type $\min(I(y))$ subject to integral constraint $J(y) =$ constant. For concreteness and simplicity, we choose the functionals $I(y) = \int_{x_0}^{x_1} F(x, y, y')\mathrm{d}x$, and $J(y) = \int_{x_0}^{x_1} G(x, y, y')\mathrm{d}x$, with prescribed fixed boundary conditions at $x = x_0$ and $x = x_1$. We have derived our results by determining the first and second variations of $I(y) + \lambda J(y)$ by expanding the function $K(\epsilon) = (I + \lambda J)(y + \epsilon\eta)$ about $\epsilon = 0$, that is, by choosing a one-parameter family of comparison functions $Y_\epsilon = y + \epsilon\eta$ (y being the extremizing functions and $\epsilon \ll 1$):

$$K(\epsilon) = K(0) + \epsilon K_1(y, \eta) + \tfrac{1}{2}\epsilon^2 K_2(y, \eta) + \cdots, \tag{B 1}$$

$$K_1(y, \eta) = \int_{x_0}^{x_1} \left(\eta F_y^* + \eta' F_{y'}^*\right) \mathrm{d}x, \quad K_2(y, \eta) = \int_{x_0}^{x_1} \left(\eta^2 F_{yy}^* + 2\eta\eta' F_{yy'}^* + \eta'^2 F_{y'y'}^*\right) \mathrm{d}x, \tag{B 2}$$

with $F^* = F + \lambda G$. If $y(x)$ is an extremizing solution, then $\mathrm{d}K/\mathrm{d}\epsilon = 0$ at $\epsilon = 0$, or

$$K_1(y, \eta) = \int_{x_0}^{x_1} \left(F_y^* - \frac{\mathrm{d}}{\mathrm{d}x} F_{y'}^*\right) \eta \mathrm{d}x = 0. \tag{B 3}$$

With arbitrary η, we obtain the Euler–Lagrange equation satisfied by $y(x)$:

$$\frac{\partial F^*}{\partial y} - \frac{\mathrm{d}}{\mathrm{d}x}\left(\frac{\partial F^*}{\partial y'}\right) = 0, \tag{B 4}$$

where the unknown Lagrange multiplier is determined by imposing the constraint $J(y) =$ constant. Then a sufficient condition for y to minimize I is $\delta^2 K \equiv \frac{1}{2}\epsilon^2 K_2(y, \eta) > 0$. Note that in § 2 we have absorbed the small parameter ϵ into η.

In order to appropriately guarantee the constraint $J(y) =$ constant, it is more appropriate for isoperimetric problems to consider (see Courant & Hilbert 1953, Chapter IV, § 7)

$$K(\epsilon_1, \epsilon_2, \lambda) = (I + \lambda J)(y + \epsilon_1\eta_1 + \epsilon_2\eta_2), \tag{B 5}$$

that is, to consider a two-parameter family of comparison functions $Y_{\epsilon_1\epsilon_2} = y + \epsilon_1\eta_1 + \epsilon_2\eta_2$. If y is an extremizing function, then $\partial K/\partial\epsilon_i = 0$ at $\epsilon_1 = \epsilon_2 = 0$ for arbitrary choice of η_1 and η_1:

$$\int_{x_0}^{x_1} \left(\eta_i F_y^* + \eta_i' F_{y'}^*\right) \mathrm{d}x = 0, \tag{B 6}$$

which leads again to equation (B 4) for both $i = 1$ and $i = 2$. Then the criterion for y to be a local minimum is found by imposing that the determinant of second partial derivatives

$$\det \begin{bmatrix} \dfrac{\partial^2 K}{\partial \epsilon_1^2} & \dfrac{\partial^2 K}{\partial \epsilon_1 \partial \epsilon_2} & \dfrac{\partial^2 K}{\partial \epsilon_1 \partial \lambda} \\ \dfrac{\partial^2 K}{\partial \epsilon_1 \partial \epsilon_2} & \dfrac{\partial^2 K}{\partial \epsilon_2^2} & \dfrac{\partial^2 K}{\partial \epsilon_2 \partial \lambda} \\ \dfrac{\partial^2 K}{\partial \epsilon_1 \partial \lambda} & \dfrac{\partial^2 K}{\partial \epsilon_2 \partial \lambda} & \dfrac{\partial^2 K}{\partial \lambda^2} \end{bmatrix}$$

evaluated at $(\epsilon_1 = 0, \epsilon_2 = 0, \lambda)$ be negative. We find

$$\frac{\partial^2 K}{\partial \epsilon_1^2} = \int_{x_0}^{x_1} \left(\eta_1^2 F^*_{yy} + 2\eta_1 \eta_1' F^*_{yy'} + \eta_1'^2 F^*_{y'y'}\right) \mathrm{d}x,$$

$$\frac{\partial^2 K}{\partial \epsilon_1 \partial \epsilon_2} = \int_{x_0}^{x_1} \left(\eta_1 \eta_2 F^*_{yy} + (\eta_1 \eta_2' + \eta_1' \eta_2) F^*_{yy'} + \eta_1' \eta_2' F^*_{y'y'}\right) \mathrm{d}x,$$

$$\frac{\partial^2 K}{\partial \epsilon_2^2} = \int_{x_0}^{x_1} \left(\eta_2^2 F^*_{yy} + 2\eta_2 \eta_2' F^*_{yy'} + \eta_2'^2 F^*_{y'y'}\right) \mathrm{d}x,$$

$$\frac{\partial^2 K}{\partial \epsilon_i \partial \lambda} = \int_{x_0}^{x_1} \left(\eta_i G_y + \eta_i' G_{y'}\right) \mathrm{d}x = \int_{x_0}^{x_1} \left(G_y - \frac{\mathrm{d}}{\mathrm{d}x} G_{y'}\right) \eta_i \mathrm{d}x,$$

$$\frac{\partial^2 K}{\partial \lambda^2} = 0.$$

Clearly, η_1 and η_2 can be rescaled such that

$$\frac{\partial^2 K}{\partial \epsilon_1 \partial \lambda} = \frac{\partial^2 K}{\partial \epsilon_2 \partial \lambda}.$$

Then we find the sufficient condition for local minimization is

$$\left(\frac{\partial^2 K}{\partial \epsilon_1 \partial \lambda}\right)^2 \int_{x_0}^{x_1} \left((\eta_1 - \eta_2)^2 F^*_{yy} + 2(\eta_1 - \eta_2)(\eta_1' - \eta_2') F^*_{yy'} + (\eta_1' - \eta_2')^2 F^*_{y'y'}\right) \mathrm{d}x > 0, \tag{B 7}$$

which is identical to our previous condition. Hence we can formally state the condition for stationarity of I subject to $J =$ constant and the condition for local minimization by considering a one-parameter family of comparison functions $y + \epsilon\eta$. Despite the fact that such a family cannot satisfy the precise constant value J^* imposed on $J(y)$, the procedure still enforces the precise form of functional J.

Appendix C. Stability criterion

We seek to determine stationary values of Q subject to the constraints (2.19) and (3.1). The first variation of functional H defined by

$$H(\eta) = Q(\eta) - \mu_0 \int_0^{\lambda} \int_{s_0}^{s_1} \eta \mathrm{d}s\, \mathrm{d}z - \mu \int_0^{\lambda} \int_{s_0}^{s_1} \eta^2 \mathrm{d}s\, \mathrm{d}z, \tag{C 1}$$

where μ_0 and μ are Lagrange multipliers, is given by

$$\begin{aligned}\delta H &= \int_0^{\lambda}\int_{s_0}^{s_1}(\eta_s\delta\eta_s+\eta_z\delta\eta_z-(\mu+\kappa^2)\eta\delta\eta-\mu_0\delta\eta)\mathrm{d}s\,\mathrm{d}z\\ &\quad+\int_0^{\lambda}(\alpha_0\eta(s_0)\delta\eta(s_0)+\alpha_1\eta(s_1)\delta\eta(s_1))\mathrm{d}z\\ &=-\int_0^{\lambda}\int_{s_0}^{s_1}(\eta_{ss}+\eta_{zz}+(\kappa^2+\mu)\eta+\mu_0)\delta\eta\mathrm{d}s\,\mathrm{d}z+\int_0^{\lambda}(\eta_s(s_1)+\alpha_1\eta(s_1))\delta\eta(s_1)\mathrm{d}z\\ &\quad+\int_0^{\lambda}(-\eta_s(s_0)+\alpha_0\eta(s_0))\delta\eta(s_0)\mathrm{d}z+\int_{s_0}^{s_1}[\eta_z\delta\eta]_{z=0}^{z=\lambda}\mathrm{d}z. \qquad (C\,2)\end{aligned}$$

With $\delta\eta$ arbitrary, we arrive at the Euler–Lagrange equation

$$\eta_{ss}+\eta_{zz}+(\kappa^2+\mu)\eta+\mu_0=0,\quad s_0\leqslant s\leqslant s_1,\quad 0\leqslant z\leqslant\lambda, \qquad (C\,3)$$

with the boundary conditions

$$\eta_s(s_1,z)+\alpha_1\eta(s_1,z)=-\eta_s(s_0,z)+\alpha_0\eta(s_0,z)=0 \qquad (C\,4)$$

$$\eta_z=0,\quad z=0,\,\lambda. \qquad (C\,5)$$

Note that μ_0 can be eliminated from (C 3) by imposing the constraint $\int\eta\mathrm{d}s\,\mathrm{d}z=0$:

$$\mu_0=\frac{1}{\lambda(s_1-s_0)}\int_0^{\lambda}(\alpha_1\eta(s_1,z)+\alpha_0\eta(s_0,z))\mathrm{d}z. \qquad (C\,6)$$

Furthermore, if (η^*,μ^*,μ_0^*) is a solution of the eigenvalue problem (C 3)–(C 5) and satisfies the constraints (2.19) and (3.1), then functional $Q(\eta^*)$ takes the value

$$\begin{aligned}Q(\eta^*)=-\int_0^{\lambda}\int_{s_0}^{s_1}(\eta^*_{ss}+\eta^*_{zz}+\kappa^2\eta^*)\eta^*\mathrm{d}s\,\mathrm{d}z+\int_0^{\lambda}(\eta^*_s(s_1)+\alpha_1\eta^*(s_1))\eta^*(s_1)\mathrm{d}z\\ +\int_0^{\lambda}(-\eta^*_s(s_0)+\alpha_0\eta^*(s_0))\eta^*(s_0)\mathrm{d}z=\mu^*. \qquad (C\,7)\end{aligned}$$

Hence we conclude that $\min(Q)=\min(\mu)$. Thus the stability of a static liquid ridge can be guaranteed if the smallest eigenvalue $\min(\mu)$ solution of (C 3)–(C 5) is positive. For a rigorous proof of this result see Courant & Hilbert (1953), Vol. I, Chapter VI.

Appendix D. Equivalent stability criterion

We first determine the variation of the pressure p as the liquid cross-sectional area A of the unperturbed meniscus is varied, *for fixed wall geometry and fixed contact angle*. For definiteness, we examine the configuration of figure 16 of a symmetric meniscus with negative–pressure:

$$p=-\frac{\sigma}{r}. \qquad (D\,1)$$

The origin O of the coordinate system is chosen such that the contact line is located at $(x,0)$. When the area A is varied by $\mathrm{d}A$, the contact line position becomes $(x+\mathrm{d}x,\mathrm{d}y)$, while the parameters r (meniscus radius), θ_0 (meniscus half-angle), ϕ (wall angle) vary by $\mathrm{d}r$, $\mathrm{d}\theta_0$, and $\mathrm{d}\phi$ respectively. With the identities

$$\phi=\theta_0+\gamma,\quad r=\frac{x}{\sin\theta_0},\quad \kappa_w=\cos\phi\frac{\mathrm{d}\phi}{\mathrm{d}x}, \qquad (D\,2)$$

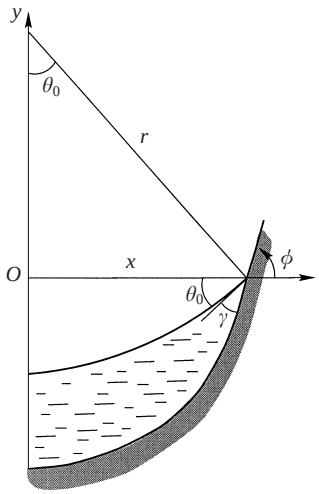

FIGURE 16. Symmetric meniscus partially wetting a solid surface with contact angle γ; ϕ denotes the angle made by the wall with the x-axis at the contact line. The curvature of the interface is such that the pressure within the liquid is $p = -\sigma/r$.

we find

$$\frac{\mathrm{d}r}{\mathrm{d}x} = \frac{1}{\sin\theta_0} - x\frac{\cos\theta_0}{\sin^2\theta_0}\frac{\mathrm{d}\theta_0}{\mathrm{d}x} = \frac{1}{\sin\theta_0}\left(1 - r\kappa_w\frac{\cos\theta_0}{\cos(\theta_0+\gamma)}\right). \tag{D 3}$$

Furthermore, to leading order of infinitesimals, the variation in A is given by

$$\mathrm{d}A = x\mathrm{d}y + O(x^2) \tag{D 4}$$

leading to, with $\mathrm{d}y = \tan(\theta_0+\gamma)\mathrm{d}x$,

$$\mathrm{d}A/\mathrm{d}x = r\sin\theta_0\tan(\theta_0+\gamma). \tag{D 5}$$

Finally, we obtain from equation (D 1)

$$\frac{\mathrm{d}p}{\mathrm{d}A} = \frac{\sigma}{r^3}\frac{\sin\gamma}{\sin^2\theta_0\sin(\theta_0+\gamma)}\left(\frac{\cos\gamma - r\kappa_w}{\sin\gamma}\cos\theta_0 - \sin\theta_0\right). \tag{D 6}$$

We then see that condition (3.17) for meniscus stability to transverse perturbations is equivalent to

$$\mathrm{d}p/\mathrm{d}A > 0. \tag{D 7}$$

The same condition applies for a positive-pressure meniscus. Condition (3.18) can be interpreted as follows. First, we note that if the meniscus is stable to infinite-wavelength transverse perturbations, then it will be stable to all shorter-wavelength perturbations. Thus the stability can be inferred in the limit of perturbations of infinite wavelength. For infinitesimal perturbations of very large wavelength λ, the cross-sections of the perturbed meniscus free surface in the planes $z = 0$ and $z = \lambda$ are nearly identical to the cross-section of the unperturbed equilibrium meniscus, that is, are nearly circles. If at $z = 0$ both pressure and cross-sectional area A are larger than at $z = \lambda$, then the liquid will flow from the thicker section $z = 0$ to the thinner section $z = \lambda$, and stability of the liquid ridge is guaranteed. Conversely, if the pressure is smaller in the thicker sections, then the perturbation will grow and the liquid ridge may break into droplets.

More specifically, assume that the perturbed meniscus region located between the planes $z = 0$ and $z = \lambda$ is partitioned into two cylindrical sections of areas $A + \mathrm{d}A_1$

and $A + \mathrm{d}A_2$ respectively. Let c be the fraction of the length along the z-axis of the partition of area $A + \mathrm{d}A_1$. Conservation of volume implies

$$c\mathrm{d}A_1 + (1 - c)\mathrm{d}A_2 = 0. \tag{D 8}$$

Then the pressure difference between the two stations $z = 0$ and $z = \lambda$ is given by

$$\mathrm{d}p_1 - \mathrm{d}p_2 = \frac{\sigma}{r^2}(\mathrm{d}r_1 - \mathrm{d}r_2) = \frac{\sigma}{r^3}\frac{\sin\gamma}{\sin^2\theta_0 \sin(\theta_0 + \gamma)}\left(\frac{\cos\gamma - r\kappa_w}{\sin\gamma}\cos\theta_0 - \sin\theta_0\right)\frac{\mathrm{d}A_1}{1 - c} \tag{D 9}$$

using (D 6). Since $0 < c < 1$, the sign of $\mathrm{d}p_1 - \mathrm{d}p_2$ is that of $\mathrm{d}A_1$ if the condition $r\alpha\cos\theta_0 > \sin\theta_0$ is satisfied by the cylindrical ridge.

REFERENCES

Brown, R. A. & Scriven, L. E. 1980 On the multiple equilibrium shapes and stability of an interface pinned on a slot. *J. Colloid Interface Sci.* **78**, 528–542.

Concus, P. & Finn, R. 1969 On the behavior of a capillary surface in a wedge. *Proc. Natl Acad. Sci. USA* **63**, 292–299.

Concus, P. & Finn, R. 1979 The shape of a pendent liquid drop. *Phil. Trans. R. Soc. Lond.* A **292**, 307–340.

Concus, P. & Finn, R. 1974 On capillary free surfaces in the absence of gravity. *Acta Math.* **132**, 177.

Concus, P. & Finn, R. 1990 Capillary surfaces in microgravity. *Prog. Aeronaut. Astronaut.* **130**, 183–206.

Concus, P. & Karasalo, I. 1978 A numerical study of capillary stability in a circular cylindrical container with a concave spheroidal bottom. *Comput. Meth. Appl. Mech. Engng* **16**, 327–339.

Courant, R. & Hilbert, D. 1953 *Methods of Mathematical Physics*, Vol. I. Interscience.

Davis, S. H. 1980 Moving contact lines and rivulet instabilities. Part 1. The Static rivulet. *J. Fluid Mech.* **98**, 225–242.

Finn, R. 1986 *Equilibrium Capillary Surfaces.* Springer.

Huh, C. & Scriven, L. E. 1971 Hydrodynamic model of steady movement of a solid-liquid-fluid contact line. *J. Colloid Interface Sci.* **35**, 85.

Karasalo, I. 1979 Stability of axisymmetric annular fluid interfaces at zero contact angle. *Arch. Rat. Mech. Anal.* **71**, 257–270.

Langbein, D. 1990 The shape and stability of liquid menisci at solid edges. *J. Fluid Mech.* **213**, 251–265.

Majumbar, S. R. & Michael, D. H. 1976 The equilibrium and stability of two-dimensional pendent drop. *Proc. R. Soc. Lond.* A **351**, 89–115.

Michael, D. H. 1981 Meniscus stability. *Ann. Rev. Fluid Mech.* **13**, 189–215.

Myshkis, A. D., Babskii, V. G., Kopachevskii, N. D., Slobozhanin, L. A. & Tyuptsov, A. D. 1987 *Low-Gravity Fluid Mechanics.* Springer.

Padday, J. F. 1969 Surface tension. Part I. The theory of surface tension. Part II. The measurement of surface tension. In *Surface and Colloid Science* (ed. E. Matijevic & F. R. Eirich), Vol. I, pp. 39–149. Wiley-Interscience.

Padday, J. F. & Pitt, A. R. 1973 The stability of axisymmetric menisci. *Phil. Trans. R. Soc. Lond.* A **275**, 489–528.

Princen, H. M. 1969 The equilibrium shape of interfaces, drops, and bubbles. Rigid and deformable particles at interfaces. In *Surface and Colloid Science* (ed. E. Matijevic & F. R. Eirich), Vol. II, pp. 1–84. Wiley-Interscience.

Sekimoto, K., Oguma, R. & Kawazaki, K. 1987 Morphological stability analysis of partial wetting. *Ann. Phys.* **176**, 359–392.

Schwartz, L. W. 1998 Hysteretic effects in droplet motions on heterogeneous substrates. *Langmuir* **14**, 3440–3453.

Schwartz, L. W. & Eley, R. R. 1998 Simulation of droplet motion on low-energy and heterogeneous surfaces. *J. Colloid Interface Sci.* **202**, 173–188.

Vogel, T. 1987 Stability of a liquid drop trapped between two parallel planes. *SIAM J. Appl. Maths* **47**, 516–525.